The many phases of massive galaxies : a near-infrared spectroscopic study of galaxies in the early universe

Kriek, M.T.

Chapter 6

The Detection of a Red Sequence of Massive Field Galaxies at $z \sim 2.3$ and its Evolution to $z \sim 0$

Abstract:
The existence of massive galaxies with strongly suppressed star formation at $z \sim 2.3$, identified in Chapter 3, suggests that a red sequence may already be in place beyond $z = 2$. In order to test this hypothesis, we study the rest-frame $U - B$ color distribution of massive galaxies at $2 < z < 3$. The sample is drawn from our near-infrared (NIR) spectroscopic survey for massive galaxies. We find a statistically significant ($> 3\sigma$) red sequence in the color distribution, which hosts $\sim 60\%$ of the stellar mass at the high-mass end. The red-sequence galaxies have little or no ongoing star formation, as inferred from both emission-line diagnostics and the stellar continuum shapes. Their strong Balmer breaks and the location of the galaxies in the rest-frame $(U - B)$, $(B - V)$ plane indicate that the star formation in these galaxies has just recently been suppressed. In order to study the evolution of the red sequence, we compare our sample with spectroscopic samples at $0.02 < z < 0.045$ and $0.6 < z < 1.0$. Rest-frame $U - B$ evolves by only ~ 0.16 mag from $z \sim 2.3$ to the present at a given mass. Over the same redshift interval, the number and stellar mass density on the high-mass end of the red sequence grows by factors of ~ 8 and ~ 6 respectively. We explore simple models to explain the observed evolution. Just aging of stellar populations predicts too strong $\Delta(U - B)$ and no evolution in the number density. More complicated models that include aging, quenching and red mergers provide reasonable fits to $\Delta(U - B)$ and the number density evolution. However, the effects of dust, which cannot be fully assessed with current data, complicate the interpretation.

Mariska Kriek, Arjen van der Wel, Pieter G. van Dokkum,
Marijn Franx, & Garth D. Illingworth
To be submitted to *The Astrophysical Journal*

6.1 Introduction

EARLY TYPE GALAXIES with quiescent stellar populations form a well-defined color-magnitude or color-mass relation at $z \sim 0$, known as the red sequence. They are clearly separated from blue star-forming galaxies, which populate a different, less-tight sequence, called the blue cloud. While the red sequence is primarily build up of massive galaxies, blue galaxies have lower stellar masses (e.g, Kauffmann et al. 2003).

The appearance and evolution of the red sequence provide a powerful method to study the star-formation and assembly history of massive galaxies (e.g., Bower et al. 1992; Schweizer & Seitzer 1992; van Dokkum et al. 1998). The red sequence exhibits a tilt and spread which are thought to be primarily driven by metallicity and age differences, respectively (e.g., Faber 1973; Worthey 1994; Kodama & Arimoto 1997; Kodama et al. 1999). Both the shape and the color of the red sequence evolve over cosmic time. Several processes are responsible for this evolution. First, the color gradually reddens due to aging of stellar populations. Second, the red sequence grows through transformations of blue galaxies. These transformations change the mix of properties of red-sequence galaxies and may cause the observed evolution of the red sequence to deviate from the expectations from passive evolution. Third, mergers among red-sequence galaxies change the red-galaxy mass function and may affect the color, slope, and scatter of the red sequence (e.g., Bower et al. 1992). Thus, the evolution of the color, the shape, the number and mass density of the red sequence sets direct constraints on the assembly and star formation history of massive early type galaxies.

The evolution of the red sequence between $z \sim 1$ and $z \sim 0$ has extensively been studied for this purpose. Overall, these studies find that the color evolution is consistent with just aging of stellar populations (e.g., Bell et al. 2004), the mass on the red sequence doubles in this redshift interval (e.g., Bell et al. 2004; Arnouts et al. 2007), and the growth at higher masses is attributed to both red mergers and galaxy transformations (e.g., Bundy et al. 2007). As a significant part of the red sequence was already in place at $z \sim 1$, we have to push our studies to higher redshift to trace the onset and first build up of the red sequence.

Recent high-redshift studies report the detection of the red sequence up to $z = 2$ (e.g., Arnouts et al. 2007). Moreover, developments in NIR instrumentation have enabled the first spectroscopic confirmations of quiescent galaxies without detected emission lines beyond $z = 2$ (see Chapters 3 and 4; Kriek et al. 2006a,b). In particular the cross-dispersed mode of the Gemini Near-Infrared Spectrograph (GNIRS, Elias et al. 2006), with a wavelength coverage of 1-2.5 μm allows systematic studies of massive galaxies at $z \sim 2.3$. Using this instrument we have completed a NIR spectroscopic study of 36 K-selected galaxies at $2 \lesssim z \lesssim 3$.

In this chapter we will use this survey to study the onset and color evolution of the red sequence. The spectroscopic redshifts in combination with the accurate continuum shapes as provided by the NIR spectra, allow for the first time accurate rest-frame color determinations of quiescent, massive galaxies beyond $z = 2$. Throughout the chapter we assume a ΛCDM cosmology with $\Omega_{\rm m} = 0.3$, $\Omega_\Lambda = 0.7$, and $H_0 = 70$ km s^{-1} Mpc^{-1}, and a Salpeter (1955) initial mass function (IMF) between 0.1 and 100 $M_\odot$. All broadband magnitudes are given in the Vega-based photometric system.

6.2 Data

The data used in this work are extracted from our NIR spectroscopic survey for massive galaxies (Chapter 5; Kriek et al. 2007b). The full sample consists of 36 *K*-bright galaxies observed with GNIRS in cross-dispersed mode (1.0–2.5 μm), between 2004 September and 2007 March (programs: GS-2004B-Q-38, GS-2005A-Q-20, GS-2005B-C-12, GS-2006A-C-6, GS-2006B-C-5 and GS-2007A-C-9). The galaxies were originally selected from the multi-wavelength survey by Yale-Chile (MUSYC, Gawiser et al. 2006; Quadri et al. 2007), which provides us with accurate optical-to-NIR ($UBVRIzJHK$) photometry. In Chapter 5 (Kriek et al. 2007b) we show that the sample is representative for a mass-limited sample at $2 < z < 3$. Further details about sample completeness, observations, reduction and extraction of the spectra can also be found in Chapter 5 (Kriek et al. 2007b).

For this work we will use the 28 galaxies within the range $2 < z_{\rm spec} < 3$. Stellar masses and other population properties are derived by stellar population modeling as described in detail in Chapters 2 and 5 (Kriek et al. 2006a, 2007b). In summary, we fit the spectra together with the broadband optical photometry by Bruzual & Charlot (2003) stellar population models, assuming an exponentially declining star formation history, solar metallicity, the Calzetti et al. (2000) reddening law and the Salpeter (1955) IMF between 0.1 and 100 $M_{\odot}$. We allow a grid of 41 values for A_V between 0 and 4 mag, 31 values for the characteristic star-forming timescale (τ) between 10 Myr and 10 Gyr, and 24 values for age (not exceeding the age of the universe). We leave redshift as a free parameter for galaxies without emission lines. Uncertainties on the stellar population properties are derived using 200 Monte Carlo simulations as described in Chapters 2 and 5 (Kriek et al. 2006a, 2007b).

Rest-frame $U - B$ colors are also determined from the best-fit stellar population models. In the same fashion as for the stellar population properties, confidence levels are derived from Monte Carlo simulations. The colors are not measured directly from the spectra, as for several galaxies the *U*-band is not covered completely by the NIR spectrum, or the *B*-band falls partly in between the *J* and *H* atmospheric windows. As our grid allows almost 30 000 different synthetic spectra, we do not expect the colors to converge to certain best-fit templates. Nevertheless, in order to examine whether using best fits may introduce systematics in the derived rest-frame colors, we directly measure the colors from the NIR spectra in combination with the optical broadband photometry. We find no systematic offset between the direct colors and those derived from the best fits.

The unique aspects of this data set are the accurate spectroscopic redshifts, rest-frame colors and masses. Although broadband photometric studies provide much larger galaxy samples, they lack the accuracy needed for this study.

6.3 A Red Sequence at $z \sim 2.3$

6.3.1 The Detection of the Red Sequence at $z \sim 2.3$

Figures 6.1a and b present rest-frame $U - B$ color versus stellar mass for the $2 < z < 3$ massive galaxy sample. The colors are corrected for redshift differences within the

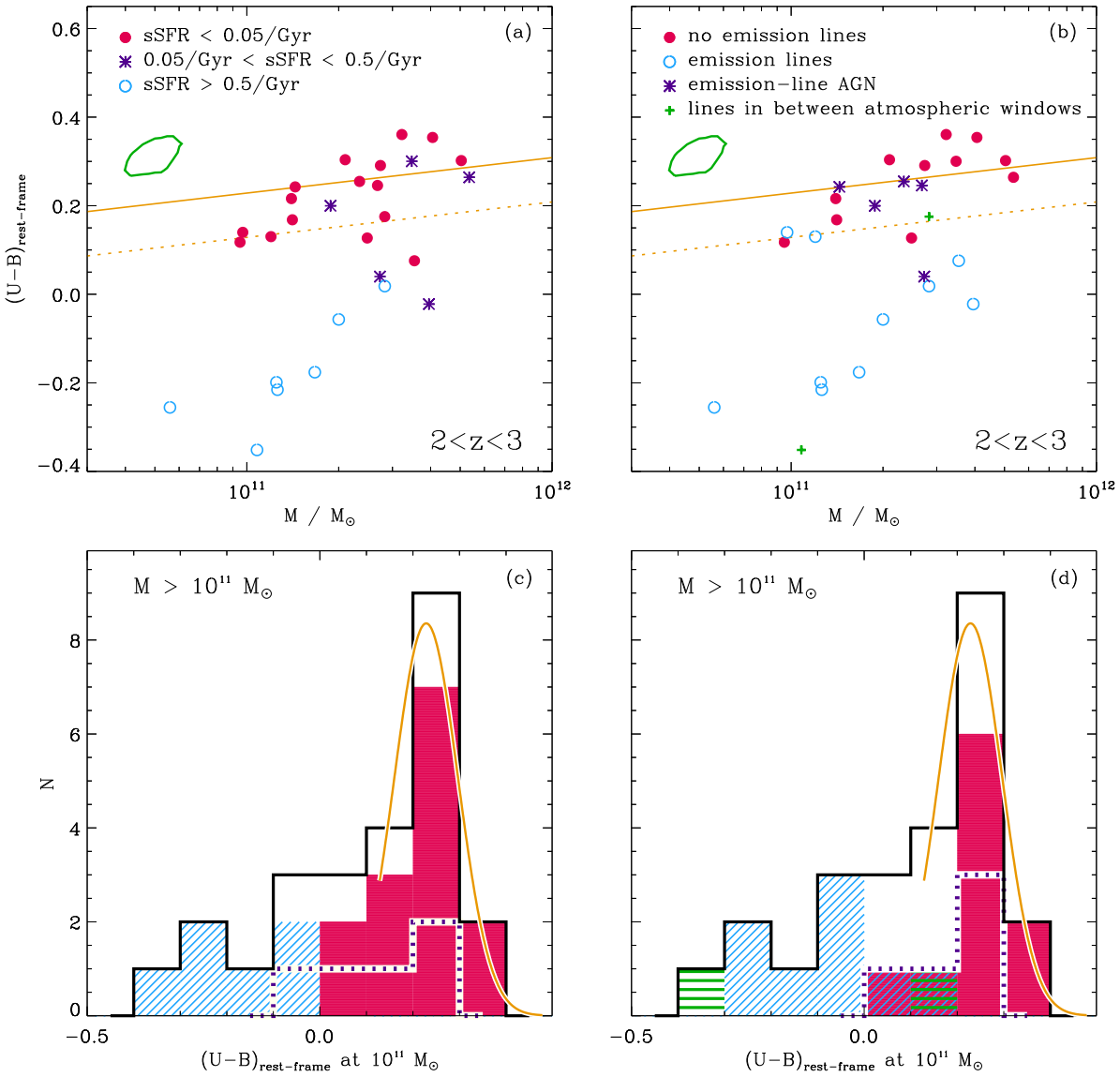

Figure 6.1 — Rest-frame $U - B$ vs. stellar mass (*top panels*) and the color distribution along the $z \sim 0.0$ slope (*bottom panels*) for the $2 < z < 3$ massive galaxy sample. The left and right panels indicate the properties of the galaxies according to SED modeling and emission line diagnostics, respectively. The black histograms in the bottom panels show a significant peak ($> 3\sigma$), indicating that a red sequence was already in place at $z \sim 2.3$. The solid curve in the bottom panels represents the best fit to the color distribution of the red-sequence galaxies. The resulting location of the red sequence is indicated by the solid line in the top panels. All galaxies above the dotted line in the top panels are defined as red-sequence galaxies in this work ($(U - B)_M > (U - B)_{\rm peak} - 0.1$). The symbols in panel *a* indicate the best-fit specific SFRs, and in panel *b* we show whether we detected emission lines for the galaxies. For the emission-line galaxies we discriminate between those for which the line emission is dominated by star formation, or by AGN activity, following the selection criteria as presented in Chapter 4 (Kriek et al. 2007a). The corresponding color distributions are presented in panel *c*, such that the solid symbols correspond to the solid histograms, the open symbols to the diagonally hatched histograms, the asterisks to the open dotted histograms and the pluses to the horizontally hatched histograms. The average 1σ confidence interval is given in the top left of the top panels. Both independent star formation indicators imply that the red sequence at $z \sim 2.3$ is dominated by galaxies with little or no ongoing star formation.

sample, as will be explained in § 6.4.2. These correction are very small (~ 0.002 mag), and barely change the appearance of this plot. The distribution of galaxies in Figures 6.1a and b is striking, as there are many galaxies with similar, red colors. In order to test whether a red sequence was already in place at this early epoch, we correct the colors for the slope of the $z = 0$ red sequence (van der Wel et al. 2007) and examine the residuals. The applied correction has the form

$$(U - B)_M = (U - B) - 0.08\,(\log M/M_\odot - 11) \tag{6.1}$$

The residuals are shown by the black histograms in Figures 6.1c and d. The distribution exhibits a conspicuous peak at $(U - B) \sim 0.25$ mag. We test the significance of the red sequence by calculating the probability to obtain this peak when assuming a flat distribution. If the true distribution is uniform the probability of finding ≥ 9 galaxies in any one of the 4 red bins is $<$0.0004, and we conclude that the detection of the red sequence is significant at the $\sim 3.3\sigma$ level. This implies that a red sequence of massive field galaxies was indeed already in place at $z \sim 2.3$.

We determine the location of the peak of the red sequence by fitting a Gaussian to the color distribution. We average over many binning positions to obtain a distribution that is not affected by the particular choice of binning. In order to avoid including blue-cloud galaxies, we restrict the fitting region to all galaxies with $(U - B)_M > (U - B)_{\rm peak} - 0.1$. Hence, this procedures requires a few iterations. The best fit is indicated by the solid curve in Figures 6.1c and d. The peak of the distribution is shown by the solid line in Figures 6.1a and b. All galaxies above the dotted line ($[U - B]_M > [U - B]_{\rm peak} - 0.1$) are defined as red-sequence galaxies from hereon.

6.3.2 Properties of Red-Sequence Galaxies

In the previous section we showed that a red sequence was already in place at $z \sim 2.3$. The well-defined shape of the red sequence could be a consequence of the converging colors of evolved galaxies. However, our sample is small, and dusty starburst galaxies, known to be highly abundant at these redshifts (e.g., Webb et al. 2006; Papovich et al. 2006), may contribute to, or even dominate the red sequence at these early epochs. In order to test whether these red-sequence galaxies indeed host quiescent stellar population, we examine the star formation properties using several diagnostics.

In Figure 6.1a the galaxies are coded following their best-fit specific SFR derived from modeling their stellar continua (see § 6.2 and Chapter 5; Kriek et al. 2007b). The corresponding color distributions are presented in Figure 6.1c. Most red-sequence galaxies are best-fit by specific SFRs less than 0.05 Gyr^{-1}, and three have specific SFRs between 0.05 and 0.5 Gyr^{-1}. The uncertainties on the specific SFRs are about a factor of ~ 3 on average (Chapter 5; Kriek et al. 2007b). Nevertheless, the large fraction of galaxies with low specific SFRs suggests that red sequence is not dominated by dusty starbursts.

A combination of two rest-frame colors, such that one isolates the optical break, and the other color measures the slope of the spectrum redwards of the optical break (e.g., Förster Schreiber et al. 2004; Labbé et al. 2005; Wuyts et al. 2007), may also be used to discriminate between dusty star-forming galaxies and quiescent stellar populations.

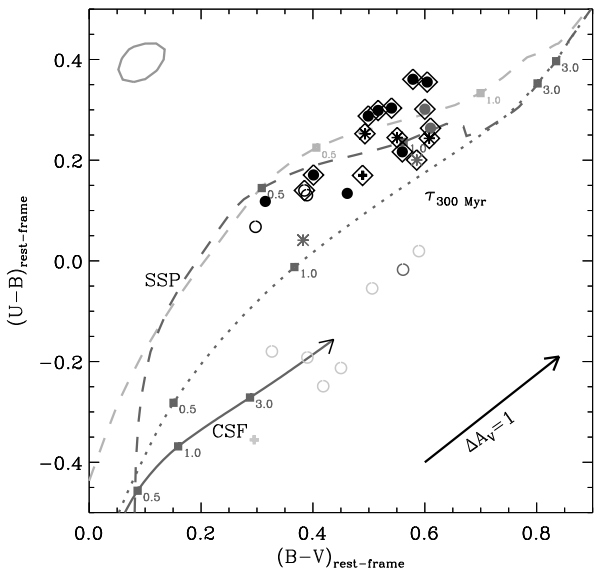

Figure 6.2 — Rest-frame $U-B$ versus $B-V$ for the $2<z<3$ massive galaxy sample. The symbols indicate the emission line diagnostics, similar as in Figure 6.1b. The colors indicate the best-fit specific SFRs similar as in Figure 6.1a, such that the open symbols, asterisks and solid symbols correspond to the light gray, dark gray and black symbols, respectively. The red-sequence galaxies are indicated by the open diamonds. The average $1\,\sigma$ confidence interval is given in the top left. The dark gray curves show the color evolution tracks of Bruzual & Charlot (2003) models for an SSP (*dashed line*), an exponentially declining model with a τ of 300 Myr (*dotted line*), and a CSF model (*solid line*), all for solar metallicity. The dashed, light-gray curve represents an SSP model with $Z=2.5Z_{\odot}$. Ages in Gyr are indicated along the tracks. The vector indicates a reddening of $A_V=1$ mag for a Calzetti et al. (2000) law. The $B-V$ colors of the red-sequence galaxies may infer a post-starburst phase.

In Figure 6.2 we show rest-frame $U-B$ versus $B-V$ for all galaxies between $2<z<3$. Color evolution tracks of Bruzual & Charlot (2003) models show that quiescent stellar populations have a different locus than dusty starbursts. As expected, the red-sequence galaxies are closer to the simple stellar population (SSP) model tracks. The remaining galaxies can roughly be divided in those that have colors more comparable to constant star forming (CSF) models with dust, and galaxies that will probably soon join the red sequence.

These results are supported by independent emission line diagnostics, presented in Figure 6.1b and d. We divide the sample according to whether emission lines are detected in the rest-frame optical spectra. Subsequently, the emission-line galaxies are sorted for the dominant origin of their line emission: using primarily emission-line ratios we identify active galactic nuclei (AGNs) and H II regions (Chapter 4; Kriek et al. 2007a). For two galaxies we have no information on the line emission as the lines are expected at wavelengths with low atmospheric transmission. 13 out of 15 red-sequence galaxies have no detected emission lines, or the line emission is dominated by AGNs.

Thus, both the stellar continua and the emission line diagnostics suggest that the red sequence at $z\sim2.3$ is dominated by galaxies with quiescent stellar populations. In particular, 7 out of 9 previously identified galaxies with strongly suppressed star formation presented in Chapter 3 (Kriek et al. 2006b) fall on this red sequence. The rest-frame $U-B$ colors of the two remaining galaxies with strongly suppressed star formation are just below the cut-off value, and their locus in Figure 6.2 is near the SSP track. Thus, they will most likely soon join the red sequence.

The rest-frame $B-V$ colors indicate that the red-sequence galaxies at $z\sim2.3$ are likely in a post-starburst phase (Figure 6.2). This is further illustrated in Figure 6.3, in which we show the stacked low-resolution spectrum of all red-sequence galaxies. For comparison we show a 3 Gyr SSP model with a prominent 4000 Å break in Figure 6.3

as well. In contrast to such old stellar populations, the optical break for the $z \sim 2.3$ red-sequence galaxies is clearly dominated by the Balmer break. Overall, our findings may imply that the massive end of the red sequence is just starting to build up at $z \sim 2.3$, and was likely not yet in place beyond $z \sim 3$. Kodama et al. (2007) drew the same conclusion by studying the stellar populations in protoclusters at $2 \lesssim z \lesssim 3$. Our work is also consistent with the study by Brammer & van Dokkum (2007) who found that in contrast to $z \sim 2.4$, red galaxies at $z \sim 3.7$ have significant UV emission and are thus still actively forming stars.

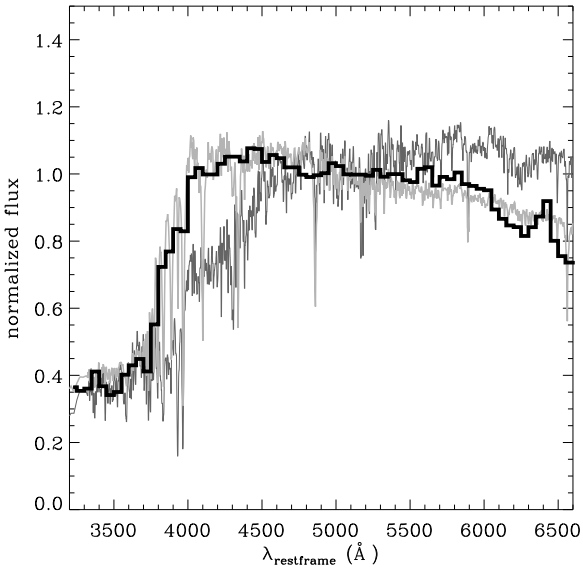

Figure 6.3 — Mean stack of the low-resolution GNIRS spectra of the red-sequence galaxies at $z \sim 2.3$ (*black curve*). Overplotted is the mean of all best-fits to the spectra in light gray. For comparison we show a 3 Gyr SSP model in dark gray. This figure shows that in contrast to the 3 Gyr model, the optical break of the stacked spectrum is dominated by the Balmer break, typical for post-starburst galaxies. This may imply that the red sequence is just starting to build up at $z \sim 2.3$.

Furthermore, Figure 6.2 provides us with a clear illustration of the different processes that may be responsible for the spread and the tilt of the red sequence at $z \sim 2.3$. $U - B$ and $B - V$ show a positive correlation for the red-sequence galaxies. The typical 1σ confidence contour shows that random errors can not fully account for the spread, and other effects are likely to play a role. The two SSP tracks, indicated by the dashed lines, show that both age and metallicity differences may be responsible for the spread and the tilt. Also the redshift spread of the red sequence galaxies, corresponding to 0.5 Gyr, will induce scatter in colors. Finally, reddening by dust moves a galaxy in a similar direction as aging and metallicity, and may also contribute to the spread and the tilt of the red sequence. The importance of the different processes can not be addressed with the current data, and independent dust, age, and metallicity constraints are required to break the degeneracies.

Finally, we stress that, although the star formation activity in the red-sequence galaxies appears low, the galaxies may still be reddened by fair amounts of dust. Best-fit stellar population models indicate an average dust content of $A_V = 0.8$ mag (using the Calzetti reddening law). However, due to degeneracies between age and dust, A_V is poorly constrained with typical uncertainties of 0.5 mag (Chapter 5; Kriek et al. 2007b), and dust-free models provide almost equally good fits to the spectra (Chapter 3; Kriek et al. 2006b). Metallicity (Z) further complicates this degeneracy, and as it is fixed to $Z_\odot$ during fitting, the lack of appropriate metallicities may have been compensated by adjusting age or A_V. Independent indicators, such as mid-infrared (MIR) imaging or Balmer decrements are needed to better constrain the dust content in these

red-sequence galaxies. MIR imaging will also reveal whether obscured starburst regions may have been missed. However, large amounts of dust seem unlikely, as that would have broadened the red sequence.

6.4 Measuring the Evolution of the Red Sequence

In order to measure the rest-frame $U-B$ evolution of the red sequence, we will compare our $z \sim 2.3$ results with those of lower redshift samples in this section. We use two spectroscopic massive galaxy samples ($> 10^{11} M_{\odot}$) at $0.02 < z < 0.045$ and $0.6 < z < 1.0$, extracted from the Sloan Digital Sky Survey (SDSS, York et al. 2000), Data Release 5 (DR5; Adelman-McCarthy et al. 2007) and the Great Observatories Origins Deep Survey (GOODS; Giavalisco et al. 2004) respectively.

6.4.1 Spectroscopic Samples at Lower Redshifts

For our lowest redshift sample we use a complete, mass-selected, volume-limited sample of galaxies at redshifts $0.02 < z < 0.045$, extracted from the SDSS. See van der Wel et al. (2007) for more details about the extraction and completeness of the sample. The SDSS $u-g$ and $g-r$ colors are used to derive rest-frame $U-B$ colors. M/L are derived from the $g-r$ colors (corrected for galactic extinction and redshift) using the relation by Bell et al. (2003). The inferred stellar masses are increased by 0.15 dex to account for differences in the IMF. The final massive ($> 10^{11} M_{\odot}$) galaxy sample consists of 903 galaxies.

For the intermediate redshift sample at $0.6 < z < 1.0$, we use a mass-selected, volume-limited galaxy sample, constructed from GOODS-south. A detailed description of the extraction of the sample and completeness can be found in van der Wel et al. (2007). rest-frame $U-B$ and $B-V$ colors for the $0.6 < z < 1.0$ sample are derived from the F606W, I775W and F850LP ACS photometry. Subsequently, $B-V$ provides us with stellar masses, using the empirical relations by Bell et al. (2003). Again, the stellar masses are increased by 0.15 dex. Of this sample, 137 galaxies have masses $> 10^{11} M_{\odot}$. Spectroscopic redshifts are known for 70% of this sample (Le Fèvre et al. 2004; Mignoli et al. 2005; van der Wel et al. 2005; Vanzella et al. 2006). As this spectroscopic sample is not fully representative for the total sample, we will include the galaxies with photometric redshifts (S. Wuyts et al. 2007 in preparation) when appropriate.

6.4.2 The Color Evolution of the Red Sequence

For an accurate measurement of the $U-B$ color evolution, it is crucial to derive the color of the red sequence in a similar fashion as for our $z \sim 2.3$ sample. In the top panels of Figure 6.4 we show rest-frame $U-B$ versus stellar mass for all three massive galaxies samples. The colors are corrected for redshift differences within each subsample, in a self-consistent way, by using the evolution of the red-sequence color with time derived below. Next, we subtract equation (6.1) from the data and determine the peak of the color distribution in the same way as was done the $z \sim 2.34$ sample. The extracted color distribution along the $z \sim 0.0$ slope is presented in the lower panels. Galaxies with colors $(U-B)_{M,z} > (U-B)_{\rm peak} - 0.1$ are defined as belonging to the red sequence. The peak locations are indicated by solid lines in Figure 6.4. For

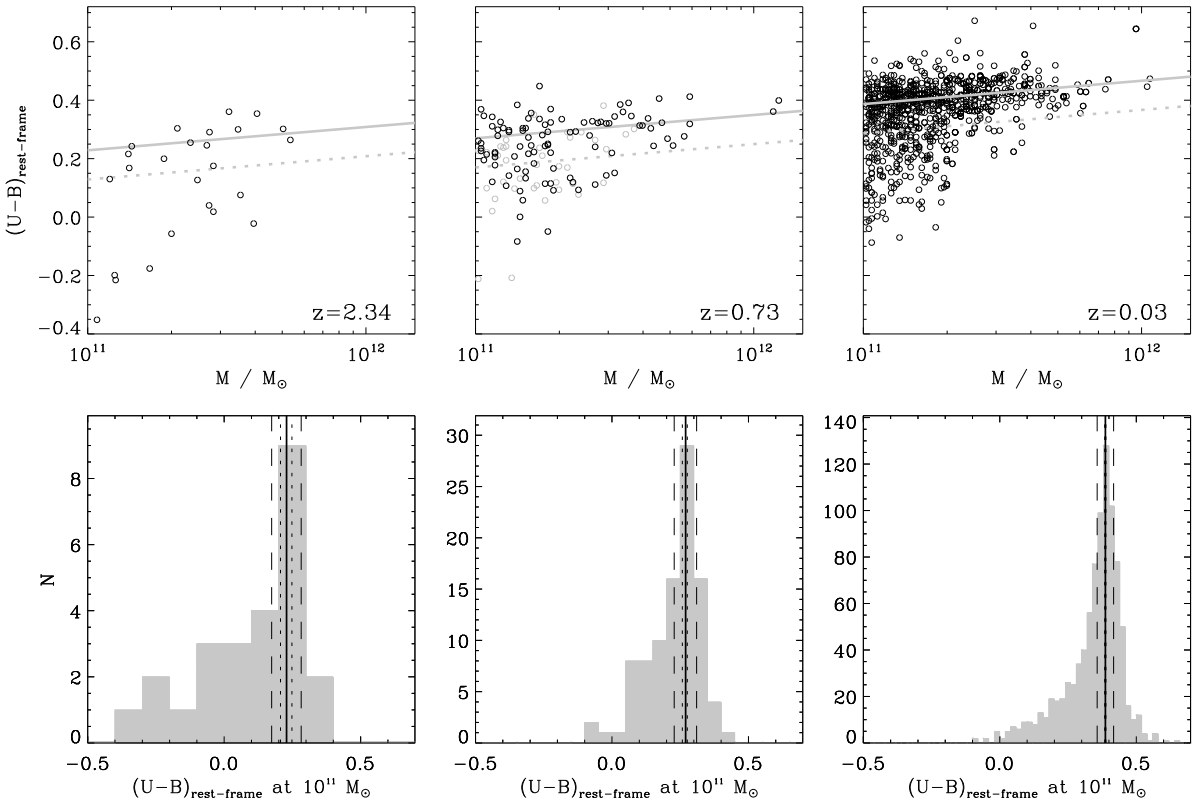

Figure 6.4 — In the top panels we show rest-frame $U - B$ color versus stellar mass for the three galaxy samples. Galaxies without spectroscopic redshifts in the $0.6 < z < 1.0$ sample are indicated in gray. The $U - B$ colors are corrected for redshift differences within the sample using equation (6.2). In the bottom panels we show the color distribution, extracted along the $z \sim 0.03$ slope (0.08 mag dex^{-1}). The peak of the red sequence is represented by the solid black and gray lines in the top and bottom panels respectively. All galaxies above the gray dotted lines in the top panels are defined as red-sequence galaxies. The dotted and dashed lines in the bottom panels indicate random and total 1σ uncertainties.

the $0.6 < z < 1.0$ galaxies we exclude the 30% without spectroscopic redshifts when deriving the peak of the red sequence, as these galaxies have less accurate rest-frame colors.

Random errors on the location of the red sequence are determined using bootstrapping, and are represented by the dotted lines in the lower panels of Figure 6.4. The use of different samples and different method to derive rest-frame colors and stellar masses may introduce additional systematic errors. In order to correctly interpret the observed evolution, we examine the following effects.

– *Aperture differences* Elliptical galaxies exhibit color gradients (e.g., Franx & Illingworth 1990). Thus, differences in the apertures that were used to measure rest-frame $U - B$ may introduce systematics in the color evolution. For both the $z \sim 0.03$ and $z \sim 0.73$ sample the rest-frame $U - B$ colors are derived for an aperture which is about equivalent to the half-light radius. For the $z \sim 2.3$ sample we use the NIR spectra to measure rest-frame $U - B$. The aperture sizes are rectangular and depend on the slitwidth (of $0\farcs675$), the extraction aperture, and extraction method. We use a weighted

(with S/N) extraction and include spatial elements that have a flux larger than 0.25 times the maximum flux (Chapter 5; Kriek et al. 2007b). Thus, the total aperture size is dependent on the light distribution of the galaxy. The average effective aperture of the $z \sim 2.34$ sample is comparable to a circular aperture of ~ 8.2 kpc.

In order to quantify possible systematics in rest-frame $U-B$ determinations of red-sequence galaxies between the $z < 1$ and $z \sim 2.3$ samples, we measure rest-frame $U-B$ for all galaxies in the $z \sim 0.73$ sample using an aperture of $1''$($\sim$7.6 kpc at $z \sim 0.73$) instead of $0\farcs5$. This aperture size is comparable to that used for the $z \sim 2.3$ sample. For the increased aperture the $U-B$ color of the $z \sim 0.73$ red sequence is 0.01 mag bluer. In order to correct for this effect, we reduce the colors of the $0.02 < z < 0.045$ and $0.6 < z < 1.0$ galaxies by 0.01 mag.

– *Zero points* Uncertainties in zero points directly result in systematic uncertainties in the derived rest-frame colors. The uncertainty on individual zero points is < 0.01 mag for both the $0.02 < z < 0.045$ [1] and $0.6 < z < 1.0$ (Sirianni et al. 2005) samples. Thus, the resulting uncertainty on $U-B$ is < 0.02 mag. For the $z \sim 2.3$ sample we use AV 0-type stars for the calibrating the spectra. This results in a uncertainty on rest-frame $U-B$ of ~ 0.03 mag. For this sample the broadband photometry provides us with an independent check on the zero points. In Chapter 5 (Kriek et al. 2007b) we find a systematic offset of ~ 0.01 mag between rest-frame $U-V$ derived from the photometry (using $z_{\rm spec}$) and the NIR spectra. This shows that the zero points probably introduce no large systematics for the $z \sim 2.3$ sample.

– *Rest-frame color determinations* The determination of rest-frame colors may also result in systematic errors. For the low and intermediate redshift samples we use the photometry in combination with spectroscopic redshifts. This method may result in systematics of ~ 0.01 mag and ~ 0.03 mag for the $0.02 < z < 0.045$ and $0.6 < z < 1.0$ samples, respectively. For the $z \sim 2.3$ sample we have higher resolution spectral shapes, provided by the NIR spectra. In the previous paragraph and in § 6.2 we discussed two tests to assess the rest-frame $U-B$ determinations, and neither of them showed significant systematics (~ 0.01 mag).

– *Stellar mass determinations* Although the stellar masses are all determined for the same IMF, the different methods used for the $z < 1$ and $z \sim 2.3$ samples may have introduced systematic errors. We tested this by determining the stellar masses for the $z \sim 2.3$ galaxies using the same method as for the lower redshift samples. This yielded stellar masses which are typically 0.14 dex less than the best-fit stellar masses. This may be due to younger and dustier stellar populations of the $z \sim 2.3$ massive galaxies. As the slope of the red sequence is 0.08 mag dex^{-1}, this may result in a systematic error of $\sim$0.01 mag on the observed color evolution. Furthermore, this effect may also alter the cut-off value of $10^{11} M_{\odot}$, and consequently the selection of massive red-sequence galaxies. Increasing the mass cut-off value by 0.14 dex would not change the peak location of the red sequence. However, the number and mass fractions of massive galaxies on the red-sequence would increase by $\sim$20% and $\sim$10%, respectively.

– *Completeness* The $z \sim 0.03$ sample is volume limited, and thus completeness effects are not expected to play a role. For the $z \sim 0.73$ sample we use just the spectro-

[1] http://www.sdss.org/

scopic subsample to estimate the red-sequence color, as photometric redshifts results in less accurate rest-frame colors. However, including all galaxies, would give a rest-frame $U-B$ color which is 0.01 mag less. Thus, completeness effects may result in a systematic error of ~ 0.01 for the $z \sim 0.73$ sample.

The $z \sim 2.34$ sample is much smaller and not volume limited. In Chapter 5 (Kriek et al. 2007b) we find that the distributions of rest-frame $U-V$ color, observed $R-K$ and $J-K$ color and redshift for the spectroscopic sample at $2 < z < 3$ are similar as for a photometric mass- and volume-limited sample at the same redshift interval. Unfortunately, we can only compare the photometric properties in order to investigate whether the subsample is representative, and thus systematics in photometric studies may jeopardize the real completeness. For example, in Chapter 5 (Kriek et al. 2007b) we identified systematics between photometric redshift and SED type, such that dusty, young galaxies were generally placed at too high redshifts. As these dusty galaxies scattered to lower redshift, they are not included in the sample used in this work. Dusty galaxies with $2 < z_{\rm spec} < 3$ may not be properly represented in the sample, as they were initially placed at too high redshift. Although this possible incompleteness may not alter our findings of the color of the red sequence, it should be kept in mind that the sample may not be complete and representative for the total population of $2 < z < 3$ galaxies. We estimate that completeness effects may result in a systematic error of ~ 0.03 mag on the rest-frame $U-B$ color of the $z \sim 2.3$ red sequence.

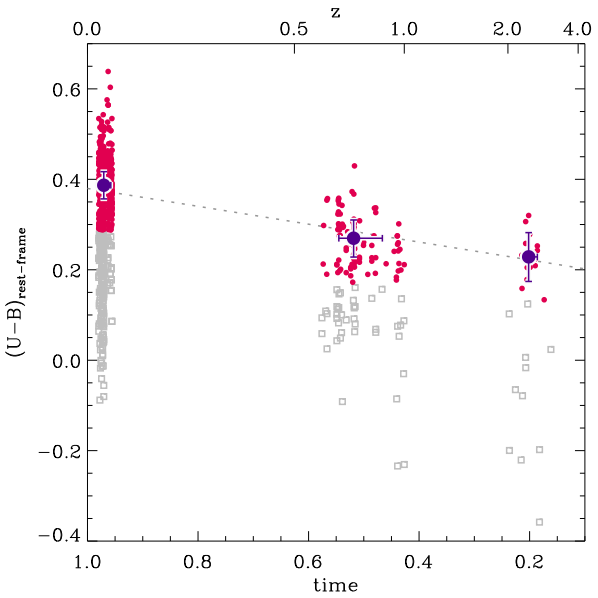

Figure 6.5 — $U-B$ color versus time for all galaxies in the three massive galaxy samples ($> 10^{11} M_{\odot}$). The rest-frame $U-B$ colors for the individual galaxies in this plot are corrected for the slope in the $U-B$ vs. stellar mass relation (0.08 mag dex^{-1}), and given for a stellar mass of $10^{11} M_{\odot}$. The red-sequence galaxies are indicated by the small filled dots, and the gray open squares represent the remaining galaxies. The colors of the red sequence for the three samples are indicated by the big filled symbols. The gray dotted line represents the best linear fit through the red-sequence locations. This relation is used to correct $U-B$ colors for redshift differences within the samples.

The various effects discussed above result in total systematic uncertainties of 0.03, 0.04 and 0.05 mag for the $z \sim 0.0$, $z \sim 0.7$ and $z \sim 2.3$ red-sequence colors respectively. We assume that the random and systematic errors are independent and can be added in quadrature.

The color evolution of massive galaxies is shown in Figure 6.5. The small filled dots show individual red-sequence galaxies, and the large filled symbols with errorbars show the peak locations for galaxies on the red sequence. The dotted line is a simple

linear fit to the large symbols, of the form:

$$(U-B)_z = 0.17 + 0.23\,t \tag{6.2}$$

with t the fractional age of the universe. The fit was used to apply differential color corrections to account for redshift differences within each sample (see above), and provides a remarkably good fit.

Table 6.1 lists the rest-frame $U-B$ color and the width of the red sequence for the three samples. The color of the red sequence evolves slowly, by $\sim$0.16 mag between between $z \sim 2.3$ and $z \sim 0.0$. In § 6.5 we will attempt to explain this evolution using simple models.

6.4.3 Evolution of the Mass and Number Density

In addition to $\Delta(U-B)$, the evolution of the number and mass density of red-sequence galaxies places constraints on the build up of the red sequence. The densities for the $z < 1$ samples follow directly from the used samples, as both are volume limited. To obtain the relative fractions at $z \sim 0.73$ we use the full $0.6 < z < 1.0$ sample, including galaxies with photometric redshifts, in combination with the red-sequence location as derived from the spectroscopic sample.

The galaxies at $2 < z < 3$ do not form a complete sample. We use the MUSYC deep survey (1030, 1256 and HDF-South, Quadri et al. 2007) to estimate the total number of massive galaxies ($> 10^{11} M_\odot$) at $2 < z < 3$ (see § 6.2). Note that most galaxies of our spectroscopic sample are extracted from this survey. We correct the obtained density for systematics in photometric redshifts as derived in Chapter 5 (Kriek et al. 2007b). We find a total number density of massive galaxies of $\rho\ (M > 10^{11} M_\odot) = 2.0 \times 10^{-4}$ Mpc^{-3}. This value is consistent with the value found by van Dokkum (2006) of $2.2^{+0.6}_{-0.6} \times 10^{-4}$ Mpc^{-3} for the same mass-cut and IMF. Subsequently we use the mass and number fractions, as estimated from the spectroscopic sample to derive the mass and number densities of red-sequence galaxies. We find a number density of massive red-sequence galaxies at $z \sim 2.3$ of $1.1^{+0.4}_{-0.4} \times 10^{-4}$ Mpc^{-3}.

Table 6.1 — Properties of the Red Sequence ($> 10^{11} M_\odot$)

	$z \sim 0.03$	$z \sim 0.73$	$z \sim 2.34$
Slope (dex^{-1})	0.08[a]	0.08[b]	0.08[b]
$U-B$ at $10^{11} M_\odot$	$0.39^{+0.03}_{-0.03}$	$0.27^{+0.04}_{-0.04}$	$0.23^{+0.05}_{-0.05}$
$\sigma_{(U-B)}$	$0.048^{+0.004}_{-0.002}$	$0.049^{+0.014}_{-0.001}$	$0.068^{+0.009}_{-0.009}$
$N_{\rm RS}$ / $N_{\rm total}$	$0.77^{+0.02}_{-0.01}$	$0.70^{+0.04}_{-0.04}$	$0.56^{+0.12}_{-0.12}$
$M_{\rm RS}$ / $M_{\rm total}$	$0.78^{+0.02}_{-0.01}$	$0.76^{+0.03}_{-0.04}$	$0.62^{+0.09}_{-0.14}$
ρ_N (10^{-4} Mpc^{-3})	$8.92^{+1.45}_{-1.45}$	$7.38^{+2.80}_{-2.79}$	$1.11^{+0.41}_{-0.41}$
ρ_M ($10^8\ M_\odot$ Mpc^{-3})	$1.63^{+0.27}_{-0.26}$	$1.35^{+0.51}_{-0.51}$	$0.26^{+0.08}_{-0.08}$

[a] Adopted from van der Wel et al. (2007)
[b] $z \sim 0.03$ slope assumed

All number and mass densities are given in Table 6.1. The uncertainties on the fractions are determined by bootstrapping (see § 6.4.2). For the number and mass densities, the uncertainties include cosmic variance, random errors, uncertainties on the fractions, and uncertainties introduced by different mass estimators. The *fraction* of the total massive galaxy population that is on the red sequence has evolved by only $\sim$ 40% from $z \sim 2.3$ to the present.

Similarly, the fraction of the total stellar mass in galaxies with $M > 10^{11} M_{\odot}$ that is on the red sequence has evolved by $\sim 25\%$. However, the total number and total mass of red sequence galaxies has increased by factors of ~ 6 and ~ 8 respectively over this time.

6.5 Modeling the Evolution of the Red Sequence

In the previous section we derived the evolution of rest-frame $U - B$ color and the number density for the massive end ($> 10^{11} M_{\odot}$) of the red sequence between $z \sim 2.3$ and the present. In this section we attempt to explain this evolution using simple models.

6.5.1 Aging of Stellar populations

The red-sequence galaxies at $z \sim 2.3$ have no or very little ongoing star formation and thus are expected to evolve passively over time. Therefore, simple aging of stellar populations seems the most straightforward explanation for the observed color evolution. In Figure 6.6a we compare the measured $U - B$ color evolution to single burst models (Bruzual & Charlot 2003) with different formation redshifts. Although IMF and metallicity affect the absolute colors, they will barely change the evolution. Therefore, the observed colors are set to zero at $z \sim 0.0$.

Figure 6.6a shows that only models with high formation redshifts may provide reasonable fits to the observed evolution. This seems in contradiction to our previous results (§ 6.3), that the star formation in the $z \sim 2.3$ red-sequence galaxies has just recently been suppressed ($\sim$0.5-1.0 Gyr). Perhaps more importantly, this model does not predict any evolution in the density of galaxies on the red sequence, in clear conflict with the observations (see solid curve in Fig. 6.7). Therefore, the evolution of the red sequence is more complicated than just aging. In the following sections we will discuss different processes that may have flattened the color evolution.

6.5.2 Growth of the Red Sequence

Not all galaxies stop forming stars at high redshift, and the red sequence will be constantly supplemented by newly quenched galaxies. Galaxies that move to the red sequence at later times will be bluer than the galaxies that already reside on the red sequence, and subsequently will flatten the total color evolution. This effect is known as the progenitor bias (van Dokkum & Franx 2001). Qualitatively, such models can reduce the apparent color evolution even though there is rapid density evolution and a constant influx of relatively young galaxies to the red sequence.

We apply a simple model in order to test whether including progenitor bias can explain the observed evolution. We assume a formation period of 100 Myr around $z_{\rm form}$ in which all galaxies are formed. The individual galaxies are quenched at $t_{\rm stop}$, following the probability distribution of $\tau_{\rm stop}$:

$$P(t_{\rm stop}) \propto \exp(-t/\tau_{\rm stop}) \tag{6.3}$$

We use Bruzual & Charlot (2003) models to construct the composite evolution from the color evolution of individual galaxies. We simulate 10 000 galaxies and determine the

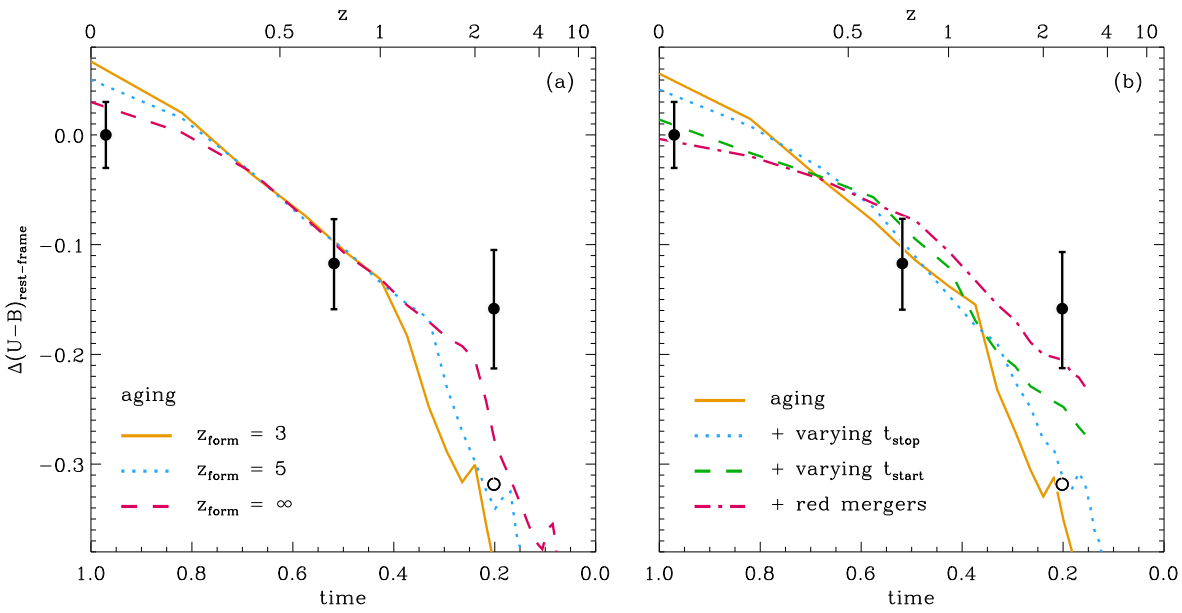

Figure 6.6 — In this figure we attempt to explain the observed rest-frame $U-B$ color evolution of the red sequence by comparison with simple models. In panel (a) we examine whether the observations are consistent with passive evolution. We show three SSP models (Bruzual & Charlot 2003) with different formation redshifts. The evolution is reasonably well-fitted by a SSP model with $z_{\rm form}=\infty$. However, this is irreconcilable with our result that the red-sequence galaxies at $z\sim 2.3$ are in a post-starburst phase. In panel (b) we examine more complicated models. The dotted curve represents a model in which newly quenched galaxies are constantly joining the red sequence. The galaxies have the same $t_{\rm start}$, but a different burst length. In the model represented by the dashed line we vary $t_{\rm start}$ as well. So for this model, galaxies are constantly formed and quenched. In the model represented by the dashed-dotted line the evolution is further flattened due to red mergers. To match our observations, all models have a minimum formation redshift such that on average the red-sequence galaxies at $z\sim 2.34$ have stopped forming stars for 1 Gyr. The combination of all effects provides a reasonable fit to the observed data. However, the unknown dust content in the $z\sim 2.3$ red-sequence galaxies complicates this interpretation. The open symbol represents the color of the $z\sim 2.3$ red sequence, corrected for the median best-fit A_V.

red-sequence color using the same method as used for the data (see § 6.4.2), we assume a constant SFR between $t_{\rm start}$ and $t_{\rm stop}$.

In Figure 6.6b we examine whether the supply of newly quenched galaxies can explain the observed $U-B$ evolution. The dotted curve represents the evolution for a constant quenching model ($\tau_{\rm stop}=\infty$). The formation time has been set such the $z\sim 2.3$ red-sequence galaxies have stopped forming stars for $\sim$1 Gyr. This model reduces $\Delta(U-B)$ compared to just aging (solid line), but neither matches the observed color evolution. However, Figure 6.7 shows that this model provides a good fit to the observed number density evolution.

The color evolution can be further reduced by varying $t_{\rm start}$ in addition to $t_{\rm stop}$. The probability distribution of the formation time of the galaxies is defined as

$$P(t_{\rm start}) \propto \exp(-t/\tau_{\rm start}) \tag{6.4}$$

The dashed curve in Figure 6.6b represents the model with constant formation and quenching rates ($\tau_{\rm start}=\infty$ and $\tau_{\rm stop}=\infty$). Also for this model we assume a mini-

mum formation redshift such that on average red-sequence galaxies at $z \sim 2.3$ have quenched their star formation 1 Gyr ago.

Although this model provides a better fit to $\Delta(U-B)$ than the previous two models, it predicts too much evolution in the number density (see Fig. 6.7). In order for this model to fit the number density evolution, the characteristic timescales $\tau_{\rm start}$ and $\tau_{\rm stop}$ should be shorter. However, this would provide a less well fit to the color evolution.

6.5.3 Red Mergers

Mergers on the red sequence may also alter the color evolution (e.g., Bower et al. 1998). Assuming that no star-formation is triggered or other major processes take place, merging of two red sequence galaxies will increase the stellar mass, but leave the color unchanged. Thus red galaxy mergers will shift the red sequence to higher masses, and consequently flatten the color evolution when measured at fixed mass.

The dashed-dotted curve in Figure 6.6b represents the color evolution when including red mergers, in addition to aging and a varying $t_{\rm start}$ and $t_{\rm stop}$. We assume a constant merger rate, normalized such that red-sequence galaxies experience one equal mass merger between $z \sim 1$ and the present. Figure 6.6b shows that the combined model provides a reasonable fit to the observed evolution.

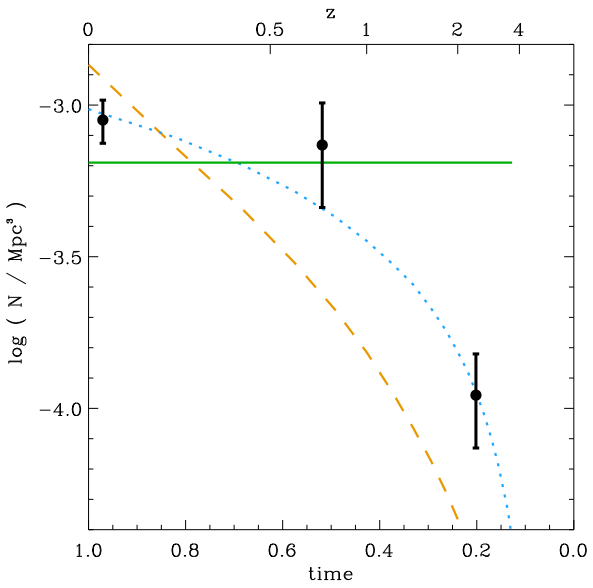

Figure 6.7 — The evolution of the number density of red-sequence galaxies more massive than $10^{11}\,M_{\odot}$ (for a Salpeter IMF). The evolution tracks correspond to the models in Figure 6.6b. Simple aging models (*solid curve*) do not match the evolution. The observed evolution is well fitted by models with a large value for $\tau_{\rm stop}$ and small values for $\tau_{\rm form}$ (*dotted curve*), or the other way around. However, if both $\tau_{\rm stop}$ and $\tau_{\rm form}$ are large (*dashed curve*), the predicted evolution is too strong. These curves ignore the effect of red mergers on the number density evolution.

Observational evidence for red mergers (e.g., van Dokkum 2005; Tran et al. 2005; Bell et al. 2006) validates this explanation. However, the corresponding decline in the rest-frame $U-B$ color evolution in this study might be overestimated. First, our assumed merger rates between $z \sim 1$ and ~ 0 may be too high, as accurate observational constraints are still lacking. Furthermore, not all major mergers are equal mass mergers, and for example a 3:1 merger ($\Delta[U-B]$=0.020 mag) has less impact on the evolution than a 1:1 merger ($\Delta[U-B]$=0.024 mag).

The effects of red mergers on the number density evolution are difficult to estimate using the simple models presented in this work. The merger rate may be dependent on mass, and accurate mass functions are needed to understand the growth of the red

sequence due to red mergers (see Bundy et al. 2007).

6.5.4 Other Influences

Although a combination of aging, quenching, and red mergers provides a reasonable fit to data, there are other possible explanation for the slow color evolution. One major concern is the unknown dust content of red-sequence galaxies, especially at $z \sim 2.3$. The well-defined shape of the $z \sim 2.3$ red-sequence makes large dust contents implausible. However, as these galaxies recently stopped forming stars, they may still be in the process of losing their dust. The red-sequence galaxies have a median best-fit A_V of 0.8 mag. But the constraints are poor with typical 1σ errors of 0.5 mag. Furthermore, as explained in § 6.3.2, the degeneracy with metallicity may introduce an additional systematic error. An A_V of 0.8 mag corresponds to $\Delta(U-B)$ of 0.16 mag for a Calzetti et al. (2000) reddening law. We show the dust-corrected value in Figure 6.6 by the open circle. The significant shift of the $z \sim 2.3$ red-sequence color provides a much better consistency with several models. Although this high dust-content in $z \sim 2.3$ red-sequence galaxies can explain the observed evolution, independent dust constraints are needed to draw any firm conclusions.

New starbursts in red-sequence galaxies, for example triggered by mergers, may also reduce the evolution. Birnboim et al. (2007) suggest that quenched galaxies may undergo a second starburst due to gas accretion. This starburst will move the galaxies back to the blue cloud. Once the star formation is quenched for the second time, the galaxy will move again to the red sequence. Compared to just passive evolution, the galaxy will be bluer due to younger ages of the newly formed stars. In this context it is interesting to note that Labbé et al. (2007) find that episodic star forming models provide the best explanation of the evolution of the blue sequence.

Also an evolving IMF or metallicity may alter the rest-frame $U-B$ evolution of the red sequence. For example, in case metallicity is lower for galaxies that quench at later times, $\Delta(U-B)$ will be slower. However, there is no observational evidence for such an effect.

Finally, we note that the used stellar population models (Bruzual & Charlot 2003) might be incomplete, and the evolution in the models may be too strong.

6.6 Summary and Conclusions

Our recent discovery of galaxies with quiescent stellar populations beyond $z = 2$ suggests that a red sequence is already in place at these redshifts. We examined this suggestion using our NIR spectroscopic survey of massive galaxies at $2 \lesssim z \lesssim 3$. The combination of spectroscopic redshifts and detailed continuum shapes as provided by the NIR spectra, allows the first accurate rest-frame color and stellar mass determinations for a massive galaxy sample beyond $z = 2$.

The distribution of galaxies in the rest-frame $U-B$ color versus mass diagram demonstrates the existence of a red sequence at $z \sim 2.3$, with a significance of $> 3\sigma$. The red sequence hosts $\sim 60\%$ of the stellar mass at the high mass end ($> 10^{11} M_\odot$) at $z \sim 2.3$. We study the stellar populations of the red-sequence galaxies using emission line diagnostics, and stellar population modeling. The stellar continua, as provided

by the NIR spectra, of nearly all red-sequence galaxies are best-fit by specific SFRs less than 0.05 Gyr^{-1}. Furthermore, in contrast to the blue galaxies, they have no detected rest-frame optical emission lines (e.g., Hα), or the line emission is dominated by AGN activity. Thus, both independent diagnostics imply that the red sequence is dominated by galaxies with quiescent stellar populations.

By combining rest-frame $U-B$ with $B-V$, we find that the star formation in the red-sequence galaxies has just recently been suppressed ($\sim 0.5-1$ Gyr). This finding is supported by the strong Balmer break in the stacked spectrum of all red-sequence galaxies. Overall, this implies that the red sequence is primarily driven by post-starburst galaxies at this epoch, and has just started to build up at $z \sim 2.3$.

We study the rest-frame $U-B$ color evolution of massive galaxies by comparing our sample with spectroscopic galaxy samples at $z \sim 0.03$ and $z \sim 0.73$. Remarkably, rest-frame $U-B$ evolves slowly, by only ~ 0.16 mag between $z \sim 2.3$ and the present. The fraction of massive galaxies ($> 10^{11} M_{\odot}$) on the red sequence increases by only $\sim 40\%$ between $z \sim 2.3$ and $z \sim 0.0$. Similarly, the fraction of the total stellar mass of massive galaxies on the red-sequence increases by only $\sim 25\%$. However, the number and mass density of the massive ($> 10^{11} M_{\odot}$) red-sequence galaxies grows by a factor of ~ 8 and ~ 6 over the same redshift interval.

Overall, we show that the slow color evolution of the red sequence does not allow a straightforward explanation. Presumably, the evolution is a combination of aging, red mergers, newly quenched galaxies and an evolving dust content of red-sequence galaxies. Simple passive aging of galaxies formed at $z \sim 7$ or beyond is ruled out, both because of the post-starburst nature of the $z \sim 2.3$ galaxies and because such models cannot reproduce the strong density evolution of galaxies on the red sequence that we measure here. The spread (σ_{U-B}) can be used to set further constraints on the build-up of the red sequence. Due to the significant errors on the rest-frame colors and the small size of the $z \sim 2.3$ spectroscopic sample, we do not use σ_{U-B} in this work. However, we note that none of the models discussed here violate the constraints imposed by the observed scatter.

As long as independent dust constraints for our $z \sim 2.3$ galaxies are missing, the color evolution is not well-suited to constrain the build-up of the red sequence. Moreover, in particular at $z < 1$ the color evolution is well fit by all models. Thus, we are dependent on the evolution of the number density and mass function for more detailed studies of the growth of the red sequence.

Acknowledgments

This research was supported by grants from the Netherlands Foundation for Research (NWO), and the Leids Kerkhoven-Bosscha Fonds. AvdW acknowledges support from NASA grant NAG5-7697. Support from National Science Foundation grant NSF CAREER AST-0449678 is gratefully acknowledged.

References

Adelman-McCarthy, J. et al. 2007, ApJ, 162, 38
Arnouts, S., et al. 2007, A&A, in press (arXiv:0705.2438)
Bell, E. F., McIntosh, D. H., Katz, N., & Weinberg, M. D. 2003, ApJ, 588, 218
Bell, E. F., et al. 2004, ApJ, 608, 752
Bell, E. F., Phleps, S., Somerville, R. S., Wolf, C., Borch, A., & Meisenheimer, K. 2006, ApJ, 652, 270
Birnboim, Y., Dekel, A., & Neistein, E. 2007, MNRAS, submitted (astro-ph/0703435)
Bower, R. G., Lucey, J. R., & Ellis, R.S. 1992, MNRAS, 254, 601
Bower, R.G., Kodama, T., & Terlevich, A. 1998, MNRAS, 299, 1193
Brammer, G., & van Dokkum, P. G. 2007, ApJ, 654, L107
Bruzual, G. & Charlot, S. 2003, MNRAS, 344, 1000
Bundy, K. Treu, T., & Ellis, R. S. 2007, ApJ, in press (arXiv:0705.1007)
Calzetti, D., Armus, L., Bohlin, R.C., Kinney, A.L., Koornheef, J., & Storchi-Bergmann, T. 2000, ApJ, 533, 682
Elias, J.H., et al. 2006, SPIE 6269, 139
Faber, S. M. 1973, ApJ, 179, 731
Förster Schreiber, N.M. et al. 2004, ApJ, 616, 40
Franx, M., & Illingworth, G.D. 1990, 359, L41
Gawiser, E., et al. 2006, ApJ, 162, 1
Giavalisco, M., et al. 2004, ApJ, 600, L93
Kauffmann, G., et al. 2003, MNRAS, 341, 54
Kodama, T., & Arimoto, N. 1997, A&a, 320, 41
Kodama, T., Bower, R. G., & Bell, E. F. 1999, MNRAS, 306, 561
Kodama, T., et al. 2007, MNRAS, 377, 1717
Kriek, M., et al. 2006a, ApJ, 645, 44
Kriek, M., et al. 2006b, ApJ, 649, L71
Kriek, M., et al. 2007a, ApJ, in press (astro-ph/0611724)
Kriek, M., et al. 2007b, ApJ, submitted
Labbé, I., et al. 2005, ApJ, 624, L81
Labbé, I., et al. 2007, ApJ, in press (arXiv/0705.3325)
Le Fèvre, O., et al. 2004, A&A, 428, 1043
Mignoli, M., et al. 2006, A&A, 437, 883
Papovich, C., et al. 2006, ApJ, 640, 92
Quadri, R., et al. 2007, AJ, 134, 1103
Rudnick, G., et al. 2001, AJ, 122, 2205
Rudnick, G., et al. 2003, ApJ, 599, 847
Salpeter, E.E. 1955, ApJ, 121, 161
Schweizer, F., & Seitzer, P. 1992, AJ, 104, 1039
Sirianni, M. et al. 2005, PASP, 117, 1049
Tran, K.-V. H., van Dokkum, P., Franx, M., Illingworth, G. D., Kelson, D. D., & Förster Schreiber, N. M. 2005, ApJ, 627, L25
van der Wel, A., Franx, M., van Dokkum, P. G., Rix, H.-W., Illingworth, G. D., & Rosati, P. 2005, ApJ, 631, 145
van der Wel, A., et al. 2007, ApJ, in press (arXiv/0707.2787)
van Dokkum, P. G., Franx, M., Kelson, D. D., Illingworth, G. D., Fisher, D., & Fabricant, D. 1998, ApJ, 500, 714
van Dokkum, P. G., & Franx, M., 2001, ApJ, 553, 90
van Dokkum, P. G. 2005, AJ, 130, 2647
van Dokkum, P. G. 2006, ApJ, 638, L59
Vanzella, E., et al. 2006, A&A, 454, 423
Webb, T.M.A., et al. 2006, ApJ, 636, L17
Worthey, G. 1994, ApJ, 95, 107
Wuyts, S., et al. 2007, ApJ, 656, 42
York, D. G. et al. 2000, AJ, 120, 1579